Electronic Supplementary Material (ESI) for Inorganic Chemistry Frontiers.

An efficient strategy to boost the directed migration of photogenerated holes by introducing phthalocyanine as a hole extraction layer

Qijing Bu,[a] Qifeng Zhao,[a] Guang Lu,[a] Xixi Zhu,[a] Yuexing Zhang,[c] Tengfeng Xie,*[b] Qingyun Liu*[a] and Jianzhuang Jiang*[d]

[a] College of Chemical and Biological Engineering, Shandong University of Science and Technology, Qingdao 266590, P. R. China

[b] College of Chemistry, Jilin University, Changchun 130012, P. R. China

[c] College of Chemistry and Chemical Engineering, Hubei University, Wuhan 430062, P. R. China

[d] School of Chemistry and Biological Engineering, University of Science and Technology Beijing, Beijing 100083, P. R. China

Surface photovoltage (SPV) spectra: SPV spectra based on lock-in amplifier were carried out on a home-made system, which is consisted of a 500 W xenon lamp (LSH-X500, Zolix), a monochromator (Omnik5006, Zolix) and a lock-in amplifier (model SR830-DSP) with an optical chopper (model SR540) running at a frequency of 23 Hz. The construction of the SPV sample cell is a sandwich-like structure of FTO/mica/sample/FTO.

SPV transient measurements: SPV transient measurements were performed on a home-made instrument. The sample was excited by the laser radiation pulse with the wavelength of 355 nm from a Nd:YAG laser ((Q-smart 450, Quantel), and the response was collected by the digital phosphor oscilloscope (TDS 5054, Tektronix). The intensity of the pulse was adjusted by a neutral grey filter and measured with a Joule meter (Starlite, Ophir, Inc.).

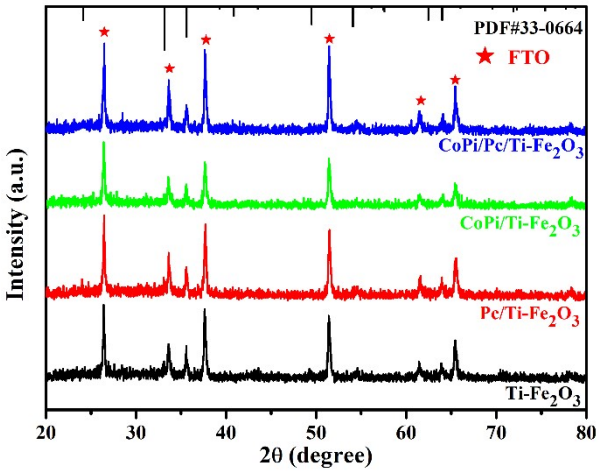

Figure S1. XRD patterns of Ti-Fe_2O_3, Pc/Ti-Fe_2O_3, CoPi/Ti-Fe_2O_3 and CoPi/Pc/Ti-Fe_2O_3.

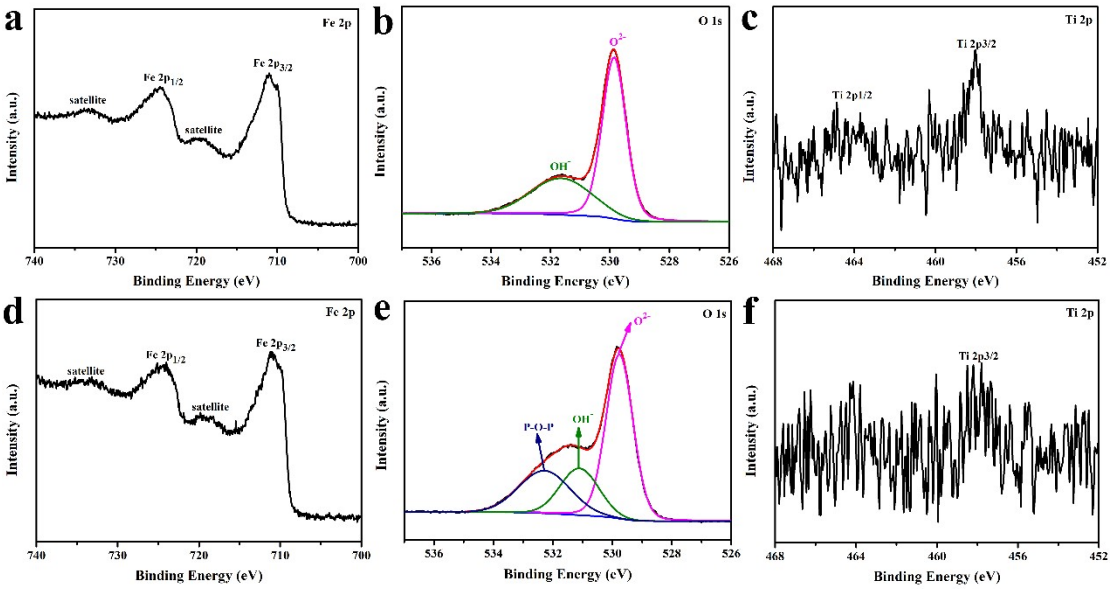

Figure S2. XPS spectra of (a) Fe 2p, (b) O 1s, (c) Ti 2p from Ti-Fe_2O_3. XPS spectra of (a) Fe 2p, (b) O 1s, (c) Ti 2p from CoPi/Pc/Ti-Fe_2O_3.

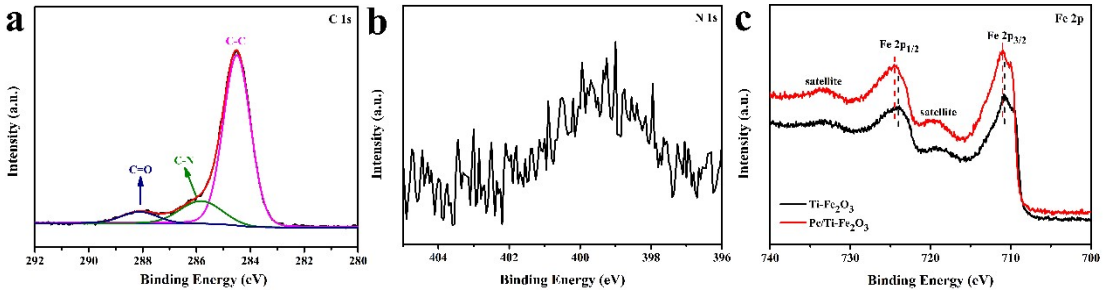

Figure S3. XPS spectra of C 1s (a) and N 1s (b) from Pc/Ti-Fe_2O_3. (c) XPS spectra of Fe 2p from Ti-Fe_2O_3 and Pc/Ti-Fe_2O_3.

The C 1s XPS spectrum is divided into three peaks at 284.5 eV, 285.9 eV and 288.1 eV, which are assigned to C-C, C-N and C=O of $H_2Pc(COOH)_8$. The N 1s XPS spectrum displays a peak at 399.5 eV, which is indexed to -NH of $H_2Pc(COOH)_8$. The binding energy of Fe 2p is shifted after the introduction of $H_2Pc(COOH)_8$, which indicates the electronic interaction between Pc and Ti-Fe_2O_3 resulted from the the chemical bonding.[1-3] The above results confirm the $H_2Pc(COOH)_8$ molecules are bonded with Ti-Fe_2O_3 sucessfully.

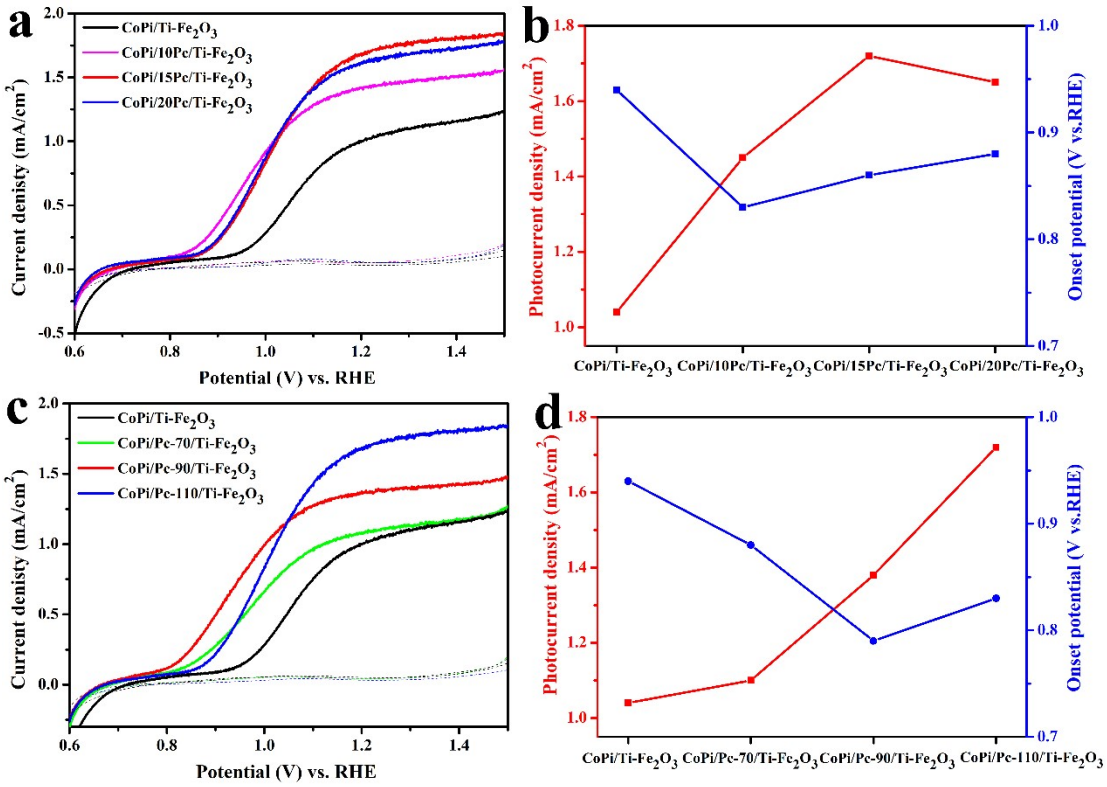

Figure S4. (a) Current density-potential (J-V) curves of CoPi/Pc/Ti-Fe_2O_3 with different concentrations of $Pc(COOH)_8$ solution. (b) Photocurrent density at 1.23 V vs. RHE and onset potential of CoPi/Pc/Ti-Fe_2O_3 with different concentrations of $Pc(COOH)_8$ solution. (c) Current density-potential (J-V) curves of CoPi/Pc/Ti-Fe_2O_3 with different temperature of hydrothermal reaction. (d) Photocurrent density at 1.23 V vs. RHE and onset potential of CoPi/Pc/Ti-Fe_2O_3 with different temperature of hydrothermal reaction.

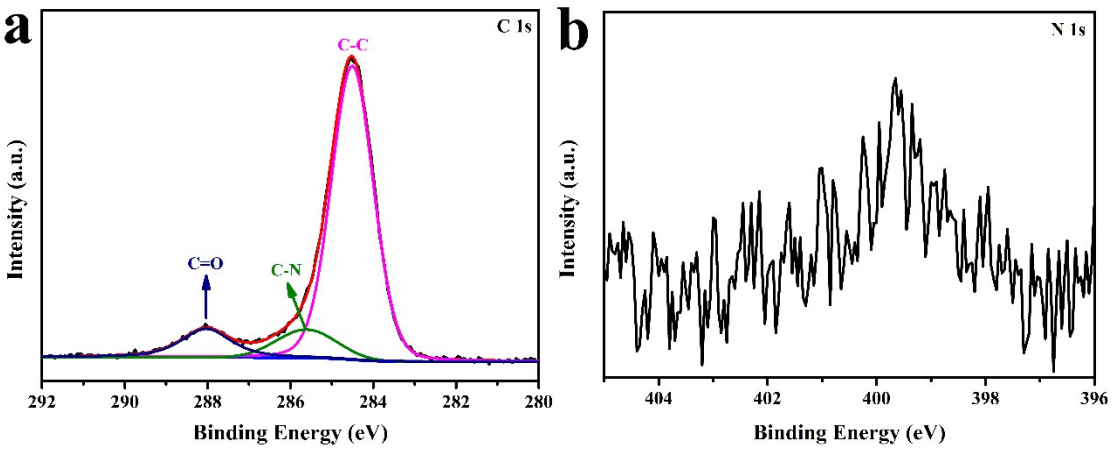

Figure S5. The XPS spectra of (a) C 1s and (b) N 1s from CoPi/Pc/Ti-Fe_2O_3 after the photostability measurement.

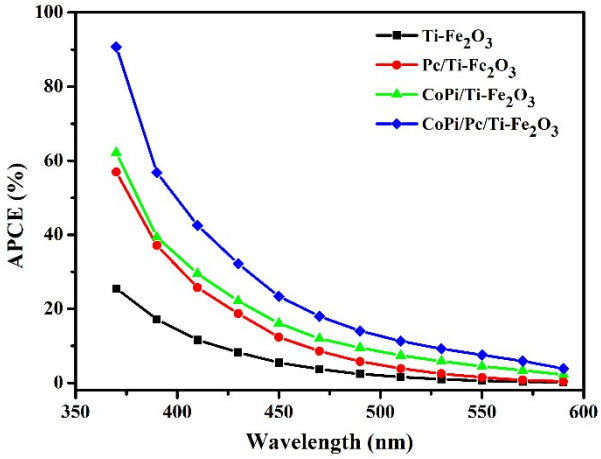

Figure S6. The absorbed photon-to-current efficiency (APCE) of Ti-Fe_2O_3, Pc/Ti-Fe_2O_3, CoPi/Ti-Fe_2O_3 and CoPi/Pc/Ti-Fe_2O_3.

The absorbed photon-to-current efficiency (APCE) was calculated according to the following equation:

$$APCE = \frac{IPCE}{LHE}$$

$$LHE = 1 - 10^{-A(\lambda)}$$

in which A(λ) is the absorbance at wavelength λ.

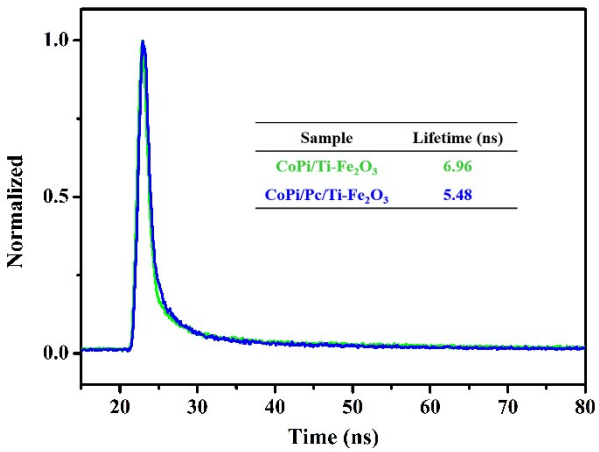

Figure S7. The time-resolved photoluminescence (TRPL) decay curves of CoPi/Ti-Fe_2O_3 and CoPi/Pc/Ti-Fe_2O_3 with an excitation wavelength of 405 nm.

Table S1. Comparison of the photocurrent density of CoPi modified Fe_2O_3 in the reported literatures with our result at 1.23 V vs. RHE under AM 1.5 G illumination

Composite	Phtocurrent density	Electrolyte	Ref
CoPi/P-Fe_2O_3	0.89 mA/cm^2	1 M NaOH	[4]
CoPi/Fe_2O_3-PN	1.6 mA/cm^2	0.1 M KOH	[5]
α-Fe_2O_3/Sb_2S_3/Co-Pi	1.14 mA/cm^2	1M NaOH	[6]
CoPi/Al_2O_3/Ti-Fe_2O_3	1.32 mA/cm^2	1 M KOH	[7]
Co-Pi/h-FeOOH/Fe_2O_3	1.31 mA/cm^2	1 M NaOH	[8]
Co-Pi/Fe_2O_3-$NaBH_4$	1.29 mA/cm^2	1 M NaOH	[9]
Fe_2O_3/R-CN/CoPi	0.7 mA/cm^2	1 M NaOH	[10]
CoPi/H_2-TiO_2/H_2-Fe_2O_3	6.0 mA/cm^2	1 M KOH	[11]
Fe_2O_3/FeB/CoPi	1.9 mA/cm^2	1 M NaOH	[12]
CoPi/Co_3O_4/Fe_2O_3	2.7 mA/cm^2	1 M KOH	[13]
CoPi/Ag/Fe_2O_3	4.68 mA/cm^2	1 M NaOH	[14]
CoPi/Pc/Ti-Fe_2O_3	1.72 mA/cm^2	1 M KOH	In this work

Table S2. Theoretical calculation results about HUMO and LOMO of $Pc(COOH)_8$

	Orbital energy (eV)	Molecular orbital diagrams
LUMO+3	-2.27	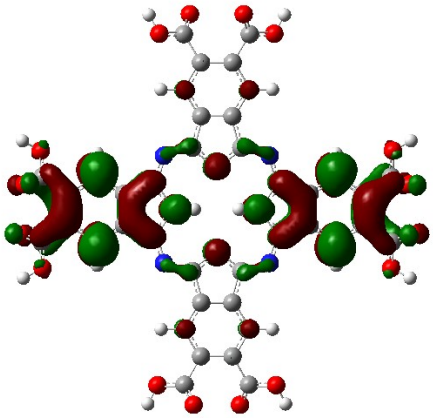
LUMO+2	-2.77	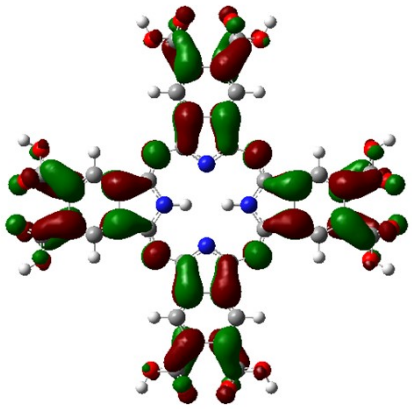
LUMO+1	-4.05	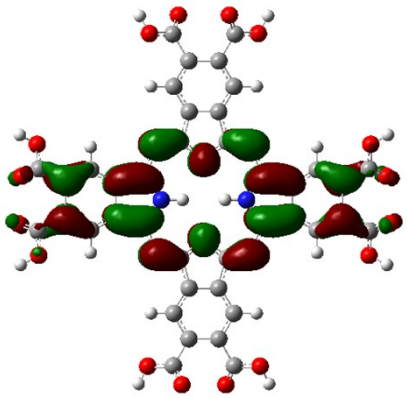

LUMO	-4.08	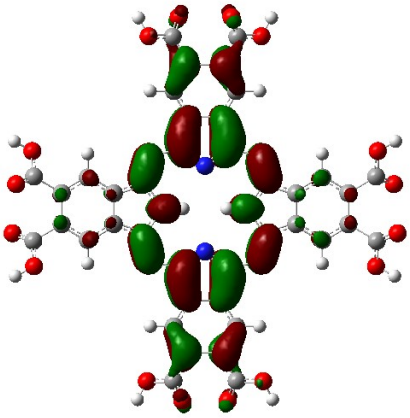
HOMO	-6.18	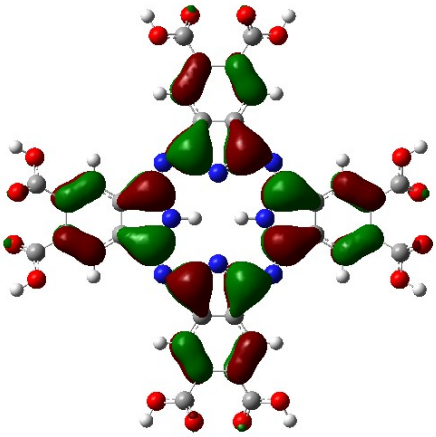
HOMO-1	-7.61	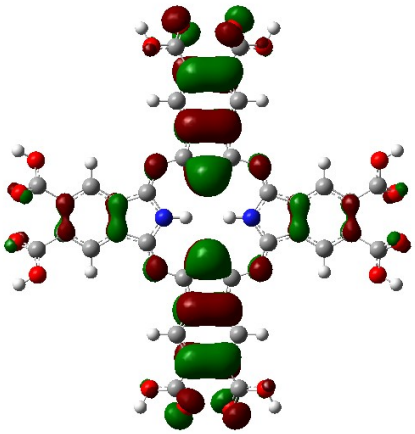

HOMO-2	-7.63	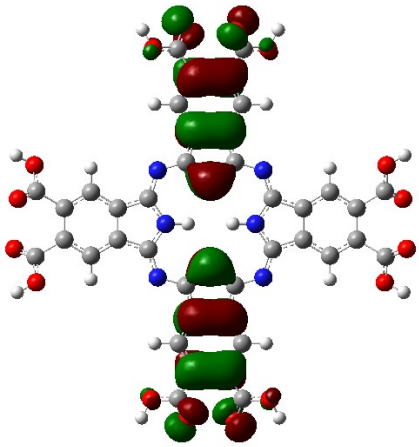
HOMO-3	-7.84	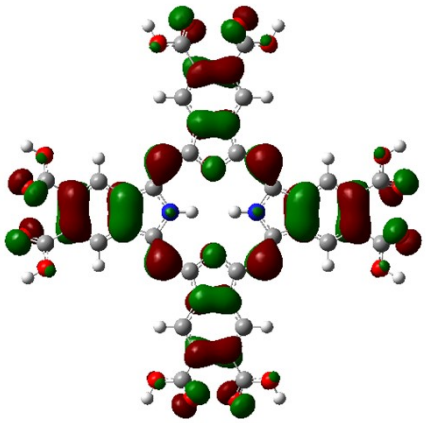

Table S3. The binding mode geometry of Ti-Fe_2O_3 and $Pc(COOH)_8$

Binding energy (kcal/mol)	Multiple perspective structure
-21.71556571	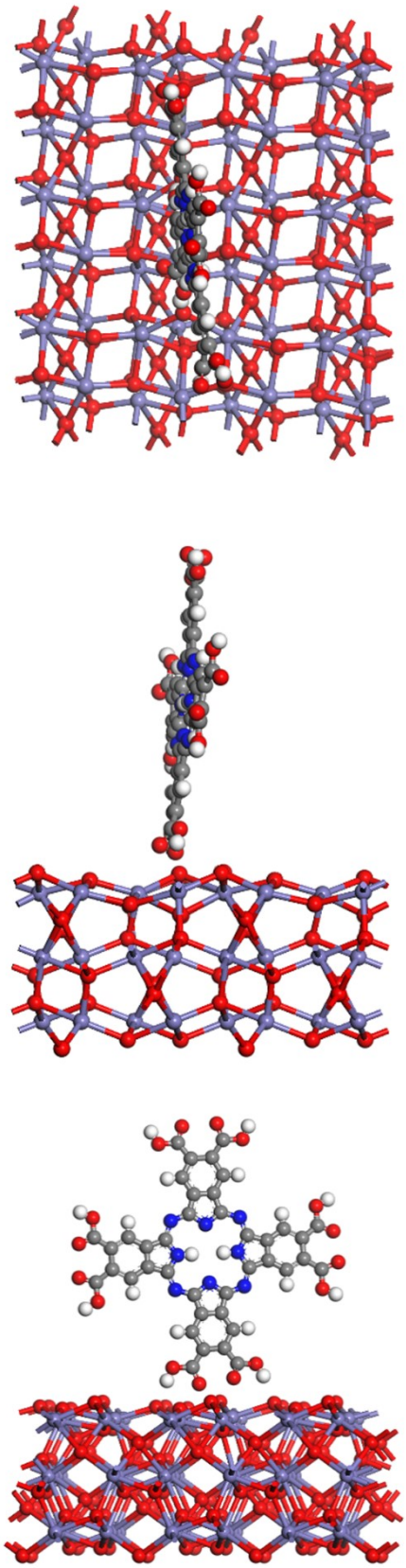

-22.03046060	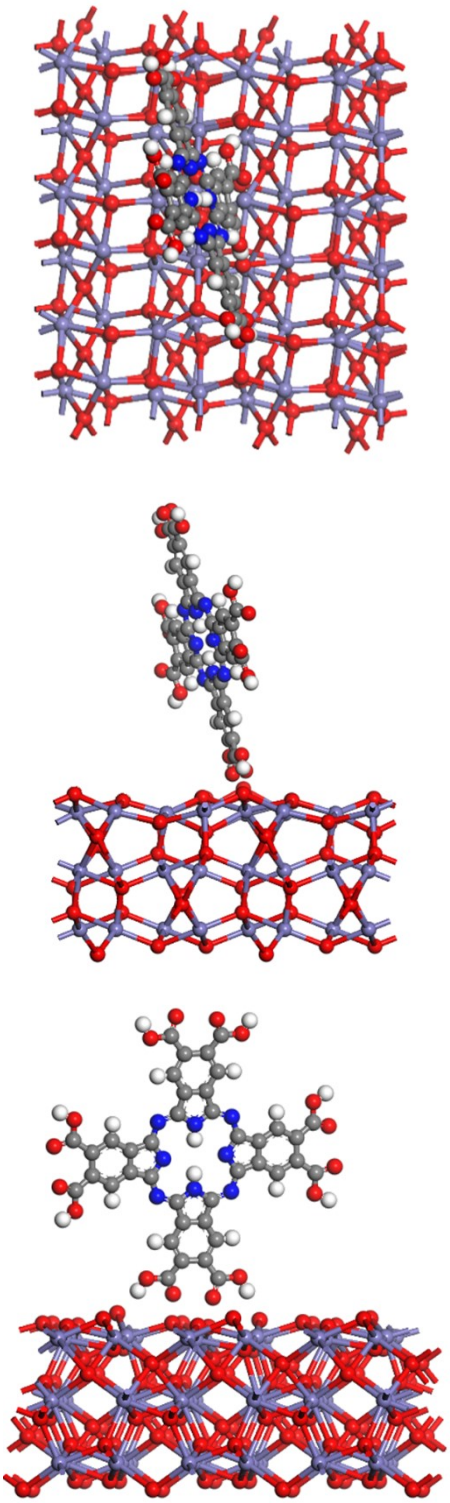

-17.80578118	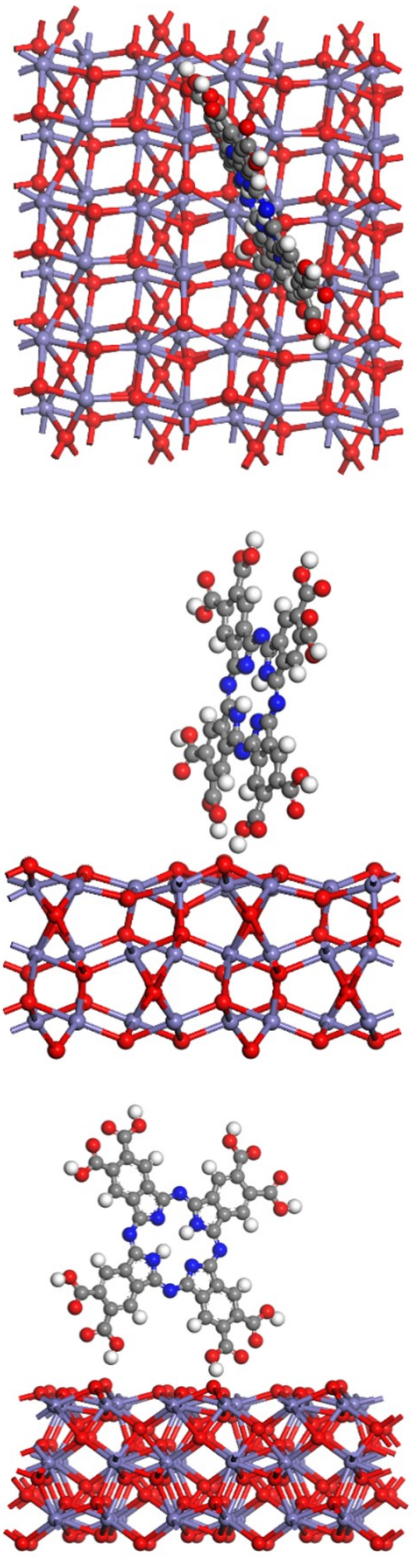

-77.95679623	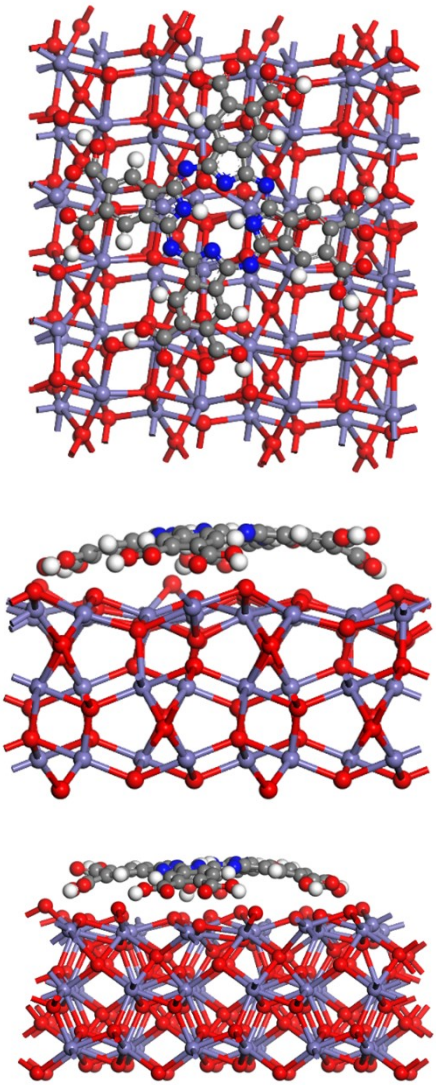

Table S4. The fitted resistances of Ti-Fe_2O_3, Pc/Ti-Fe_2O_3, CoPi/Ti-Fe_2O_3 and CoPi/Pc/Ti-Fe_2O_3 photoanodes

Sample	R_{ct1} (Ω)	R_{ct2} (Ω)
Ti-Fe_2O_3	556.6	3151.0
Pc/Ti-Fe_2O_3	169.6	758.1
CoPi/Ti-Fe_2O_3	139.2	648.1
CoPi/Pc/Ti-Fe_2O_3	136.2	481.3

REFERENCE

(1) Yu, M.-M.; Wang, C.; Li, J.; Yuan, L.; Sun, W.-J. Facile fabrication of CuPp-TiO_2 mesoporous composite: An excellent and robust heterostructure photocatalyst for 4-nitrophenol degradation. *Appl. Surf. Sci.* **2015,** *342*, 47-54.

(2) Wei, M.; Wan, J.; Hu, Z.; Peng, Z.; Wang, B. Enhanced photocatalytic degradation activity over TiO_2 nanotubes co-sensitized by reduced graphene oxide and copper (II) meso-tetra(4-carboxyphenyl)porphyrin. *Appl. Surf. Sci.* **2016,** *377*, 149-158.

(3) Gao, H.; Wang, J.; Jia, M.; Yang, F.; Andriamitantsoa, R. S.; Huang, X.; Dong, W.; Wang, G. Construction of TiO_2 nanosheets/tetra (4-carboxyphenyl) porphyrin hybrids for efficient visible-light photoreduction of CO_2. *Chem. Eng. J.* **2019,** *374*, 684-693.

(4) Wu, D.; Zhang, Z. Simultaneous non-metal doping and cocatalyst decoration for efficient photoelectrochemical water splitting on hematite photoanodes. *Electrochim. Acta* **2018,** *282*, 48-55.

(5) Liu, G.; Li, N.; Zhao, Y.; Wang, M.; Yao, R.; Zhao, F.; Wu, Y.; Li, J. Porous versus Compact Hematite Nanorod Photoanode for High-Performance Photoelectrochemical Water Oxidation. *ACS Sustainable Chem. Eng.* **2019,** *7* (13), 11377-11385.

(6) Chen, D.; Liu, Z.; Zhou, M.; Wu, P.; Wei, J. Enhanced photoelectrochemical water splitting performance of alpha-Fe_2O_3 nanostructures modified with Sb_2S_3 and cobalt phosphate. *J. Alloy. Compd.* **2018,** *742*, 918-927.

(7) Xu, D.; Bu, Q.; Wang, D.; Xie, T. Enhanced photoelectrochemical water oxidation performance by altering the interfacial charge transfer path. *Inorg. Chem. Front.* **2017,** *4* (8), 1296-1303.

(8) Xiao, J.; Fan, L.; Huang, Z.; Zhong, J.; Zhao, F.; Xu, K.; Zhou, S.-F.; Zhan, G. Functional principle of the synergistic effect of co-loaded Co-Pi and FeOOH on Fe_2O_3 photoanodes for photoelectrochemical water oxidation. *Chinese J. Catal.* **2020,** *41* (11), 1761-1771.

(9) Xiao, J.; Fan, L.; Zhao, F.; Huang, Z.; Zhou, S.-F.; Zhan, G. Kinetic analysis of the synergistic effect of $NaBH_4$ treatment and Co-Pi coating on Fe_2O_3 photoanodes for photoelectrochemical water oxidation. *J. Catal.* **2020,** *381*, 139-149.

(10) An, X.; Hu, C.; Lan, H.; Liu, H.; Qu, J. Strongly Coupled Metal

Oxide/Reassembled Carbon Nitride/Co-Pi Heterostructures for Efficient Photoelectrochemical Water Splitting. *ACS Appl. Mater. Interfaces* **2018,** *10* (7), 6424-6432.

(11) Jeon, T. H.; Moon, G.-h.; Park, H.; Choi, W. Ultra-efficient and durable photoelectrochemical water oxidation using elaborately designed hematite nanorod arrays. *Nano Energy* **2017,** *39*, 211-218.

(12) Liao, A.; He, H.; Fan, Z.; Xu, G.; Li, L.; Chen, J.; Han, Q.; Chen, X.; Zhou, Y.; Zou, Z. Facile room-temperature surface modification of unprecedented FeB co-catalysts on Fe_2O_3 nanorod photoanodes for high photoelectrochemical performance. *Journal Of Catal.* **2017,** *352*, 113-119.

(13) Yi, S.-S.; Wulan, B.-R.; Yan, J.-M.; Jiang, Q. Highly Efficient Photoelectrochemical Water Splitting: Surface Modification of Cobalt-Phosphate-Loaded Co_3O_4/Fe_2O_3 p-n Heterojunction Nanorod Arrays. *A Adv. Funct. Mater.* **2019,** *29* (11), 1801902.

(14) Peerakiatkhajohn, P.; Yun, J.-H.; Chen, H.; Lyu, M.; Butburee, T.; Wang, L. Stable Hematite Nanosheet Photoanodes for Enhanced Photoelectrochemical Water Splitting. *Adv. Mater.* **2016,** *28* (30), 6405-6410.